Environmental Science & Technology

Article

pubs.acs.org/est

Processes of Zinc Attenuation by Biogenic Manganese Oxides Forming in the Hyporheic Zone of Pinal Creek, Arizona

Christopher C. Fuller*,† and John R. Bargar‡

†United States Geological Survey, Menlo Park, California 94025, United States

‡Chemistry and Catalysis Division, Stanford Synchrotron Radiation Lightsource, Menlo Park, California 94025, United States

Supporting Information

ABSTRACT: The distribution and speciation of Zn sorbed to biogenic Mn oxides forming in the hyporheic zone of Pinal Creek, AZ, was investigated using extended X-ray absorption fine structure (EXAFS) and microfocused synchrotron X-ray fluorescence (μSXRF) mapping, and chemical extraction. μSXRF and chemical extractions show that contaminant Zn co-varied with Mn in streambed sediment grain coatings. Bulk and microfocused EXAFS spectra of Zn in the biogenic Mn oxide coating are indicative of Zn forming triple-corner-sharing inner-sphere complexes over octahedral vacancies in the Mn oxide sheet structure. Zn desorbed in response to the decrease in pH in batch experiments and resulted in near-equal dissolved Zn at each pH over a 10-fold range in the solid/solution ratio. The geometry of sorbed Zn was unchanged after 50% desorption at pH 5, indicating that desorption is not controlled by dissolution of secondary Zn phases. In summary, these findings support the idea that Zn attenuation in Pinal Creek is largely controlled by sorption to microbial Mn oxides forming in the streambed during hyporheic exchange. Sorption to biogenic Mn oxides is likely an important process of Zn attenuation in circum-neutral pH reaches of many acid-mine drainage contaminated streams when dissolved Mn is present.

INTRODUCTION

The importance of Mn oxides for sequestration of metals has been widely documented.[1−4] The formation of Mn oxides in aqueous systems occurs predominantly by microbial oxidation processes at or near zones of transition from reducing to oxidizing conditions.[5] Bacteriogenic manganese oxides are commonly phyllomanganates, such as birnessite, that are highly reactive and have high affinities for sorption of a wide variety of metal ions, including zinc, nickel, lead, and uranium.[6−10] The strong sorption affinities for metals is in part due to the presence of various types of multidentate binding sites and the need to compensate for the charge deficit resulting from Mn(IV) octhaderal vacancies that comprise about one in every six octahedral positions.[6,11] The reactivity of biogenic Mn oxides has been found to influence the mobility and fate of metal contaminants in natural aquatic environments.[5,6,12,13] A mechanistic understanding of the processes of metal sorption by naturally occurring biogenic Mn oxides is needed to adequately model reactive transport, attenuation, and bioavailability of metals in contaminated surface and ground waters.

Pinal Creek, AZ, is a well-studied mine-contaminated stream, where microbial activity has been unambiguously demonstrated to produce poorly crystalline-layered Mn oxides.[14] Microbial oxidation of Mn(II) during hyporheic exchange of water between surface flow and the streambed has produced extensive coatings of Mn oxides on streambed sediments. The coatings have elevated Co, Ni, and Zn concentrations.[13] Although the Mn oxide coatings are only a few tens of micrometers thick,[14] hyporheic exchange coupled with ongoing microbial Mn oxidation was found to attenuate 20% of the Mn load and up to 70% of the Co, Ni, and Zn contaminant loads over 5 km of streamflow.[13] This site thus serves as a model for studying terrestrial biological Mn(II) oxidation, its impact on contaminant mobility, and metal−Mn interactions. In addition, the absence of significant input of dissolved Fe to Pinal Creek provides the opportunity to investigate the role of metal sorption by biogenic Mn oxides without having to account for the contribution of sorption by Fe oxides.

Significant advances have been made in characterizing the speciation of metals sorbed to abiotic Mn oxides in laboratory studies.[15−19] Recent studies have employed direct measurement techniques, such as extended X-ray absorption fine structure (EXAFS) spectroscopy, to characterize both the structure of biogenic Mn oxides[20−23] and the speciation of metals, in particular Zn, sorbed by biogenic Mn oxides produced in the laboratory[6−8,10] and natural Mn oxides.[24,25] These studies show that aqueous Zn^{2+}, in both tetrahedral and octahedral

Received: June 10, 2013
Revised: January 10, 2014
Accepted: January 24, 2014
Published: January 24, 2014

coordination with oxygen, binds to Mn(IV) vacancy sites in hexagonal birnessite forming triple-corner-sharing surface complexes with three surface oxygens surrounding the layer vacancy.[17,18] Metal sorption processes to natural biogenic Mn oxides from field locations have not been characterized to the extent as laboratory Mn oxides or other sorbent phases, notably iron oxyhydroxides.[12]

The focus of this paper is to describe the molecular-scale speciation of Zn sorbed to biogenic hexagonal birnessite forming in the hyporheic zone of Pinal Creek.[13] We evaluate the distribution and speciation of Zn sequestered by biogenic Mn oxide coatings forming on streambed sediments comprising the hyporheic zone of a mine-contaminated stream, Pinal Creek,[13,14,26] using chemical extraction, bulk and microfocused EXAFS (μEXAFS), and microfocused synchrotron X-ray fluorescence mapping (μSXRF). The reversibility of Zn sorbed to Mn oxide coatings on streambed sediments was measured as a function of pH and solid/solution ratio to test the response of attenuated Zn to changes in streamwater chemistry. This study is the first to our knowledge to characterize the molecular-scale speciation of Zn sorbed to biogenic Mn oxides actively forming in the hyporheic zone of a mine-contaminated stream.

Site Description. Metal contamination in Pinal Creek, AZ, has resulted from infiltration of acidic water into the alluvial aquifer from Cu mining operations in the watershed 20 km upgradient of the perennial stream.[27] The acidic groundwater has reacted with minerals in the aquifer to form a neutralized contaminated groundwater plume (pH 5.5−6.5) with elevated dissolved Mn, Co, Ni, and Zn of up to 1.5 mM, 20 μM, 25 μM, and 25 μM, respectively, but very low dissolved iron.[28] Discharge of this contaminated groundwater forms the perennial stream, where the water table intersects the land surface and contributes up to 50% of streamflow at the basin outlet 5 km downstream.[26]

Previously, we characterized biogenic manganese oxides forming on Pinal Creek streambed sediments. SEM images and μSXRF maps of sediments from the hyporheic zone indicate extensive grain coatings of Mn oxides of up to 50 μm thickness.[14] On the basis of bulk and microfocused synchrotron X-ray diffraction (XRD) and EXAFS measurements, the Mn coatings are dominated by nanoparticulate Ca-bearing c-disordered hexagonal birnessite (10 Å phyllomanganate), indicative of a biogenic origin. Calculation of Mn(IV) octahedral occupancy in phyllomanganate sheets averaged 85%, consistent with one vacancy per six octahedral positions found in bio-oxides produced in pure cultures.[21,22] Weak or absent basal plane (001) reflections in XRD patterns indicate minimal or no stacking of Mn oxide layers. Consistent with this observation, XRD and transmission electron microscopy (TEM) measurements suggest that the oxides consist of nanoparticulate plates averaging 11 nm thick and 35 nm in diameter, with individual particles of very few or single layers.

EXPERIMENTAL SECTION

Streambed sediment samples analyzed in this paper are a subset of those described in our previous paper[14] that were collected from the active hyporheic zone of Pinal Creek at two sites (R2B and Z9a) 1 and 1.5 km downstream of the reach where the metal contaminated groundwater plume discharges into the stream. Sampling sites, collection, and processing were previously described.[14,29] Water chemistry for the overlying streamwater and shallow groundwater (1 m) below the streambed was similar at the two sites (see Table SI-1 of the Supporting Information). Stream water at the sampling locations (see Table SI-1 of the Supporting Information) was undersaturated with respect to hydrozincite (log SI of −9.5), the Zn solubility limiting phase in this pH range.[30] Uncontaminated, background sediment devoid of Mn coatings was collected from the dry bed of the uncontaminated ephemeral stream channel about 1 km upstream of the head of perennial flow and contaminated groundwater inflow.

Sediments at the two sites were sampled from the upper 3 cm of the streambed and sieved to <1 mm in the field using ambient streamwater.[29] A streambed push core was also collected at R2B using a push corer.[13] The 3−6 cm depth interval was used for thin sections in this study. Subsamples of surface sediments were air-dried for partial and total chemical extraction and preparation of thin sections. The core interval and background sediments were dry-sieved to <1 mm. Magnetic minerals were separated from the <1 mm dried sediments and analyzed separately because of their elevated bulk Zn concentration. Mn oxide coatings were recovered from the bulk streambed surface samples by physical abrasion of wet sediments to minimize contribution of non-contaminant Zn contained in the underlying, background minerals (see the Supporting Information). The recovered coatings were used for bulk XAS measurements and Zn desorption experiments.

Double-polished petrographic thin sections (30 μm thickness) were prepared by Spectrum Petrographics, Inc. from resin mounts (3M Scotchcast) of magnetic and non-magnetic fractions of air-dried streambed sediments (<1 mm).[14]

Metal concentrations of streambed sediments (<1 mm) and abraded coatings were determined by partial chemical extraction using 0.1 M hydroxylamine HCl in 0.05 N HNO_3 (HH) at room temperature for 1 h. This extraction scheme was effective in dissolving Mn oxides from Pinal Creek sediments.[13] Total metal concentrations were determined following total dissolution of separate sediment samples using HF−HNO_3 digestion. The resulting extraction and total dissolution sample solutions were analyzed by inductively coupled plasma−optical emission spectroscopy (ICP−OES).[13]

The reversibility of Zn sorption to the Pinal Creek biogenic Mn oxides was tested in batch suspensions of the abraded Mn oxide coatings in artificial streamwater (ASW) (see the Supporting Information), at three solid/solution ratios (solid concentration) to simulate the response of Zn attenuated in the streambed to possible inflow of more acidic water to Pinal Creek from the alluvial aquifer. The pH of the abraded coating suspension was incrementally adjusted downward from pH 7 to 4 (see the Supporting Information). After equilibration at each pH to attain constant dissolved Zn (24 h), subsamples were collected for dissolved and HH-extractable metal content.

The speciation of Zn sorbed to Pinal Creek Mn oxides was compared to Zn sorbed to biogenic Mn oxides produced using spores of *Bacillus* sp. strain SG-1. The Mn oxides were produced by culturing spores from *Bacillus* sp. strain SG-1[20] but with the addition of dissolved Zn as $ZnCl_2$ to yield Zn/Mn molar ratios of 1:100 and 1:10 (see the Supporting Information).

Bulk EXAFS, μSXRF, and μEXAFS Measurements. Bulk Zn K-edge EXAFS spectra of the isolated sediment coatings, the Zn-bearing SG-1 bio-oxide, Zn mineral specimens, and aqueous Zn(II) species were collected at the Stanford Synchrotron Radiation Lightsource (SSRL) beamline 11-2 with a Si 220 monochronomator crystal. μSXRF elemental maps (10 keV) and Zn K-edge μEXAFS spectra of streambed

sediment thin sections were collected at the Advanced Light Source beamline 10.3.2 X-ray microprobe.[31] Zn K-edge EXAFS fluorescence spectra were collected at points with elevated Mn and Zn concentrations identified in μSXRF maps. Details of XAS data collection and data analysis are presented in the Supporting Information.

RESULTS AND DISCUSSION

Sediment Chemistry. Mn-oxide-coated sediments were black, in contrast to background sediments, which ranged from buff to brown depending upon mineralogy. The <1 mm fraction of streambed sediment samples is predominantly sand-size material with less than 1 wt % of particles of <125 μm diameter. Sediments consist primarily of quartz, felspsar, illite, mica, and chlorite, along with magnetic minerals, primarily magnetite and illmenite.[32] The magnetic fraction comprised 7 and 15 wt % of the Z9a and R2B streambed sediment samples, respectively. The total Fe content of the magnetic fraction accounts for nearly all (~98%) of the total Fe in the sediment (see Table SI-2 of the Supporting Information).

A comparison of partial chemical extraction (HH) of streambed sediments from the contaminated stream reach with the background sediment shows a 5−25-fold increase in Mn, Zn, Co, and Ni concentrations (see Table SI-2 of the Supporting Information). In particular, the easily extractable component defined by the HH extraction accounts for a majority of the increase in these metals in the contaminated sediments relative to the uncontaminated, background sediment. The HH extraction of contaminated bulk sediment accounts for more than 80% of the total Mn content determined by total dissolution compared to 7% of the uncontaminated sediment. Zn in HH extractions is 15% (R2B) and 24% (Z9a) of the total Zn but only 3% for the uncontaminated sediment. Assuming that HH primarily dissolves Zn associated with the coatings, the remainder of Zn is contained within more resistant mineral components. For example, the HH-insoluble magnetic mineral fraction of Z9a sediments contains 28% of the total Zn.

HH extraction of the isolated coatings dissolved all of the Mn and >95% of the other contaminant metals (Zn, Co, Cu, and Ni) (see Table SI-2 of the Supporting Information). Assuming that the HH-extractable Mn concentration of the bulk sand is from the coatings, the coatings are estimated to comprise 2.8 and 3.0% of the bulk R2b and Z9a sediment mass, respectively. The Zn/Mn molar ratio in the coatings agrees well with the ratio in HH extraction of the bulk sediment, suggesting that the material removed by abrading is the same as the material removed by HH extraction. The Mn oxide content of the coatings is about 20 wt %, assuming a stoichiometry of MnO_2. Organic material, such as microbial cell material, comprised 3% of the mass.[14] The remainder of the material is comprised of clays[14] and other fine-grained sediment particles entrained within the coating and water. Using secondary ion mass spectrometry, Best et al. determined that Fe in Pinal Creek sediment coatings was not spatially correlated with Mn but, instead, existed as discrete particles.[32] An upper limit of 3% of the total Zn in the coatings was estimated for the fine-grained magnetic minerals by multiplying the total Fe measured in coatings by the ratio of Zn/Fe measured in the magnetic sand fraction. Similarly, an upper limit of 10% Zn in the coatings from aluminosilicate minerals was estimated by multiplying the coating Al content by the Zn/Al ratio of the uncontaminated bulk sediment. Thus, Zn measured in coatings is largely associated with the Mn oxide phases.

Contaminant Metal Distribution. μSXRF maps illustrate the distribution of metals in and on streambed sediment grains. Mn primarily occurs as coatings on sand grains of the non-magnetic mineral fraction (Figure 1), consistent with the HH extraction. Zn co-varies with Mn in the coatings but is also present in the interiors of some grains (Figure 1C). The close association of Zn with Mn is further illustrated by the high correlation of Zn and Mn in grain coatings that have little Zn or Mn within the underlying mineralogy, such as quartz grains (Figure 1B). Zn is also present in Mn oxide coatings on the magnetic mineral fraction, although high Zn concentrations are evident within magnetic mineral grains (see Figure SI-1 of the Supporting Information).

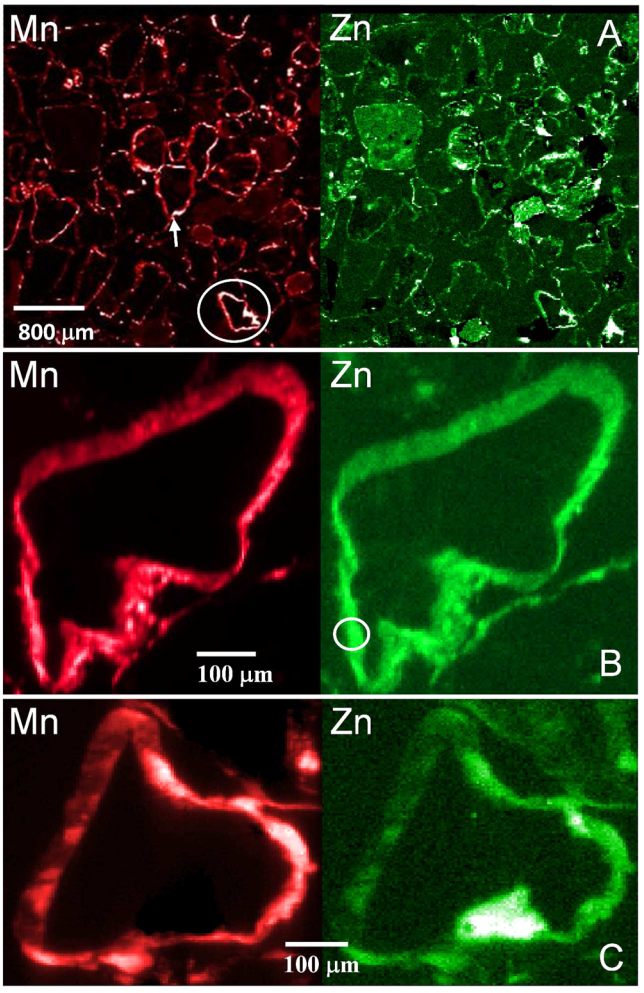

Figure 1. Zn and Mn distribution from μSXRF mapping of thin sections of non-magnetic mineral fractions of hyporheic zone sediments from sites (A and B) R2B and (C) Z9a. Brighter areas are higher concentrations. Circled grain (R2B grain 1) in panel A is shown in panel B as a higher resolution map, in which the grain orientation is rotated 90° clockwise from panel A. The white circle in panel B depicts the location of the Zn μEXAFS spectrum R2B grain 1 point 1. The arrow in panel A points to the location of the Zn μEXAFS spectrum R2B grain 2 point 3.

Mn oxide coatings are absent from the background sediments, consistent with the small fraction of the total Mn and Zn that was HH-extractable. Instead, Zn and Mn are only

dx.doi.org/10.1021/es402576f | Environ. Sci. Technol. 2014, 48, 2165−2172

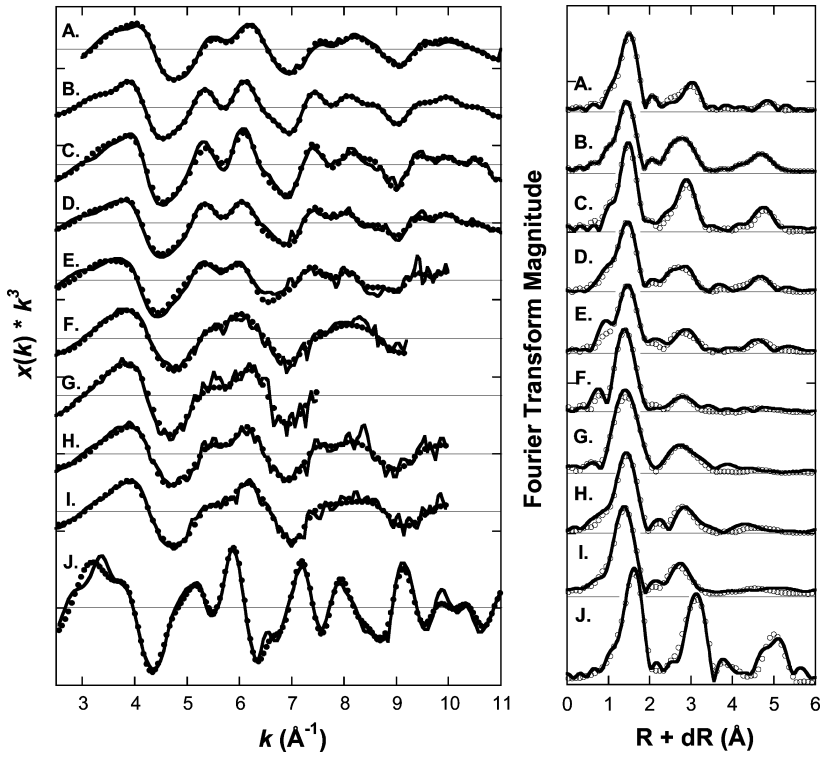

Figure 2. Zn EXAFS spectra and FTs of Pinal Creek samples (solid lines). Fits are represented by circular symbols. Spectrum A, SG-1 bio-oxide; spectrum B, R2B bulk coatings (wet); spectrum C, R2B bulk coatings (dried); spectrum D, Z9a bulk coatings; spectrum E, Z9a bulk coatings after desorption at pH 5; spectrum F, R2B non-magnetic grain 1 point 1; spectrum G, R2B non-magnetic grain 2 point 3; spectrum H, R2B magnetic grain 1 point 1; and spectrum I, R2B magnetic grain 3 point 3. Spectrum J is the chlacophanite model compound; its shell-by-shell fit is presented in Table SI-5 of the Supporting Information.

observed within the minerals of the sand-sized grains, in particular, in the magnetic fraction.

In combination, the μSXRF maps and chemical extraction results support the hypothesis that ongoing Mn oxide formation in the hyporheic zone enhances attenuation of Zn in Pinal Creek.[13] The co-distribution of Zn and Mn in the streambed sediment coatings from the contaminated reach of the stream likely is the result of microbial Mn oxidation and sequestration of contaminant Zn from streamwater during hyporheic exchange. The presence of Zn within the underlying minerals of the sediment from the contaminated stream reach represents the background or non-contaminant Zn and accounts for about 80% of the total Zn in the bulk sediment.

Local Molecular Structure of Sorbed Zn. Zn EXAFS spectra for Pinal Creek samples are generally similar to one another, the Zn-sorbed SG-1 bio-oxide, and chalcophanite (Figure 2). The chalcophanite FT peak positions are somewhat shifted compared to the samples because of a greater abundance of tetrahedral Zn (Zn_{TET}) in the samples (*vide infra*). The sample spectra are different from those of hydrozincite, zincite, smithsonite, and hetaerolite (see Figure SI-2 of the Supporting Information), Zn phases not found in Pinal Creek sediments.[32] Zn spectra of coatings also differ from Zn sorbed to hydrated alumina or iron oxides.[33,34] All Pinal Creek Zn EXAFS spectra as well as those for Zn-sorbed SG-1 Mn bio-oxides are dominated by a Zn−O pair correlation in the Fourier transforms (FTs) at ca. 1.5 Å uncorrected for phase shift (R + dR), which corresponds to a real-space Zn−O distance of ca. 1.97 Å. This distance is characteristic of tetrahedral Zn coordination.[6,15] In contrast, the longer Zn−O distance present in the FT for chalcophanite (ca. 1.7 Å, R + dR; Figure 2) indicates an octahedral environment (Zn_{OCT}). This qualitative comparison suggests that Zn exhibits dominantly tetrahedral coordination in Pinal Creek Mn oxides.

The Zn EXAFS spectra also show strong pair correlations between 2.8 and 3 Å, R + dR, and at ca. 4.8 Å, R + dR (Figure 2). The exact position and shape of these frequencies vary from sample to sample, indicating the presence of variations in the local structure around Zn. It is likely that these pair correlations contain contributions from Mn and O atoms within the hexagonal birnessite substrates. Pinal Creek Mn oxides grow in biofilms produced by Mn(II) oxidizing bacteria for surface attachment.[14] Thus, Zn may also be bound to biopolymers; i.e., the 2.8−3 Å correlations (Figure 2) could contain contributions from organic ligands. Toner et al. showed that Zn added to biofilms containing Mn oxides was sorbed onto the Mn oxide component at ratios of Zn/Mn < 0.37, with no evidence of Zn binding to organic matter.[6] In comparison, Zn/Mn ratios in Pinal Creek coatings are 0.01 (R2B and Z9a) and 0.06 in the SG-1 bio-oxide, suggesting that complexation by organic matter should be negligible. Indeed, adequate fits were obtained using only O and Mn shells. Organic ligands were subsequently neglected in EXAFS fitting. Zn−Mn frequencies in the observed distance range suggest that ZnO_4 and MnO_6 polyhdra share corners and are qualitatively consistent with a high degree of order resulting from binding of Zn as tridentate complexes over Mn octahedral vacancies observed in previous studies (see Figure SI-3 of the Supporting Information).[6,15,16]

A shell-by-shell fitting approach was used to model the EXAFS spectra. Details are described in the Supporting Information. Both tetrahedral and octahedral Zn environments were assumed to be present.[6,16,35] The coordination number

(CN) for each complex was fixed to a value of 4 for Zn_{TET} and 6 for Zn_{OCT}. To decrease the number of varied parameters and increase the robustness of the fit, the relative proportion of each type of Zn complex was floated with the Zn_{OCT} coordination number scaled by a floated parameter f_{OCT} and the Zn_{TET} coordination was scaled by $(1 - f_{OCT})$. This procedure ensured that the total effective coordination number for the Zn−O shell would remain between 4 and 6 and accounted for amplitude reduction from destructive interference by oxygens in the two subshells.[22] Best fits (Figure 2 and Table SI-3 of the Supporting Information) indicate that streambed sediment bulk coatings and the SG-1 bio-oxides contain on average 80% Zn_{TET} and 20% Zn_{OCT}, despite a 6-fold variation in the Zn/Mn ratio, equivalent to an effective overall Zn−O CN of 4.4 (3.2 for Zn_{TET} and 1.2 for Zn_{OCT}). A similar proportion of Zn_{TET} (70%) and Zn_{OCT} (30%) was found for a Zn-sorbed abiotic, synthetic hexagonal birnessite with similar Zn loading (Zn/Mn = 0.008).[16] Our results contrast, however, the finding of 100% Zn_{TET} for a biogenic Mn oxide with a Zn/Mn molar ratio of 0.07.[6] The average Zn−O tetrahedral distance at 1.97 ± 0.03 Å and the octahedral Zn−O distance of 2.17 ± 0.03 Å are in good agreement with those for Zn sorbed on abiotic birnessite[16] and a biogenic hexagonal birnessite derived in the laboratory from *Pseudomonas putida*.[6] The density functional theory shows that Zn_{TET} forms stronger bonds with O atoms surrounding the vacancy but that both Zn_{TET} and Zn_{OCT} are stable interlayer species.[18] The best fits also yield second and third shell Mn atoms at distances of 3.36 ± 0.03 and 5.39 ± 0.03 Å for Zn_{TET} and 3.53 ± 0.03 and 5.60 ± 0.03 Å for Zn_{OCT}, respectively, as expected for binding over the octahedral vacancy. Overall, the spectra provide strong evidence that sorbed Zn occurs primarily as tridentate complexes above Mn octahedral vacancies (see Figure SI-3 of the Supporting Information).

μEXAFS spectra for discrete points on sediment grain coatings of both the non-magnetic and magnetic sediment fractions all have the general features present in the bulk coating and SG-1 bio-oxide spectra (Figure 2). The higher frequency features are not as well-resolved as the bulk spectra, in part because of the limited data range of the μEXAFS. Fits yield the same Zn geometries observed in the bulk coating samples (see Table SI-3 of the Supporting Information). Individual points within the coatings exhibit a wider range of the percentage of Zn_{TET} (72−90%) but a similar average (78%) as observed in the bulk coatings and SG-1 bio-oxide (80%). The wider range of Zn_{TET} in the discrete points measured by μEXAFS may also be related to local variations, Zn/Mn ratios, or the hydration state of the sample. An important difference between the thin section samples used to collect μEXAFS spectra and the bulk samples was that drying of sediments was required for preparation of resin casts used for making thin sections. In support of this statement, we note that the dried R2B bulk coatings had a lower component of Zn_{TET} (75 ± 4%) than in the wet sample (80 ± 5%) (see Table SI-3 of the Supporting Information).

Zn Desorption. In desorption experiments with abraded coatings, the dissolved Zn concentration, [Zn], increased with a decreasing pH from pH 7 to 5 and was independent of the solid concentration over a factor of 10 range in the solid concentration (Figure 3A). The slope of log[Zn] versus pH ranged from 0.73 to 0.88 for the three conditions, yielding an average macroscopic proton stoichiometry of 1.3 H^+/mol of Zn desorbed. A decrease in slope was observed below pH 5. About 50% of the total Zn desorbed from the Mn oxides by pH 5 in the lowest solid concentration system (Figure 3B). At the pH (>6.5) of the stream, where Mn oxidation and Zn attenuation occur, very little Zn desorbed (≤0.3 μM). The observed pH dependence of Zn desorption is consistent with the pH dependence of Zn uptake by Mn oxide in lab studies.[12] Previous studies have found that Zn is reversibly sorbed to synthetic δ-MnO_2[36] and biogenic Mn oxides producing Mn-oxidizing fungus.[37]

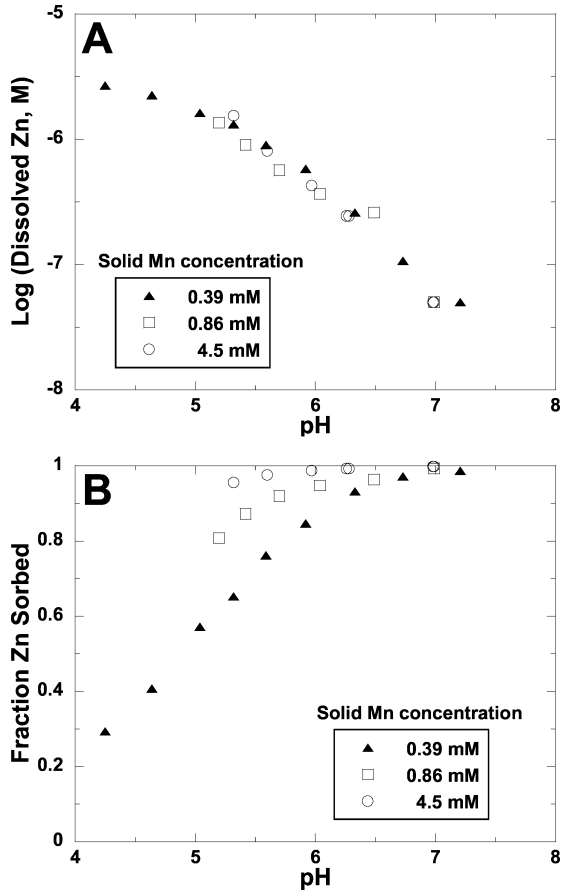

Figure 3. (A) Dissolved Zn concentration (log mol/L) released from Mn oxide coatings as a function of pH. The solid concentration is expressed as millimoles of Mn in solid per liter. (B) Fraction of remaining Zn sorbed versus pH after desorption from Mn oxide coatings.

The release of Mn also increased with decreasing pH, with the greatest release observed for the lowest solid concentration (see Figure SI-4 of the Supporting Information), with about 6% of the total Mn released at pH 4.3. By comparison, this material contains 9% Mn(II) as determined by fits of Mn K-edge X-ray absorption near edge structure (XANES).[14] It is unknown if Mn release is the result of dissolution or desorption of Mn(II) or Mn(III) bound by the hexagonal birnessite. Less than 2% of the total measured Zn desorption in each of the experimental systems can be attributed to Mn oxide dissolution assuming congruent dissolution, where Zn released is proportional to Mn release and controlled by the total Zn/Mn ratio of the solid.

The near-equal concentrations of dissolved of Zn resulting from desorption in the experiments spanning a factor of 10 range in the solid concentration could be interpreted as a solubility control for Zn. However, because Mn^{4+} is not soluble in water, birnessite dissolution as such is not possible. In the absence of reduction, mineralogic transformation of hexagaonal

dx.doi.org/10.1021/es402576f | Environ. Sci. Technol. 2014, 48, 2165−2172

birnessite was not observed between pH 7 and 5.5,[38] suggesting that Zn sorption is likely not affected by structural changes to the Mn oxide in response to the pH decrease. Furthermore, Zn−Mn distances indicative of incorporation into the Mn oxide layer are not observed, consistent with density functional theory simulations that show that Zn is unstable in the octahedral layer vacancy and, instead, is repelled out of the sheet to the more stable tridentate corner-sharing complex over vacancy.[19] Hence, Zn is not incorporated into the three-dimensional structure of the hexagonal birnessite.

Although the desorption experiments were well-below saturation with respect to hydrozincite across the experimental pH range, the presence of a secondary Zn phase that might result in the observed desorption behavior was evaluated. The local structure of the remaining sorbed Zn was determined by analysis of the Zn EXAFS spectrum of the biogenic oxide coatings, following 50% desorption at pH 5 in the lowest solids concentration system. Fitting of this spectrum yielded the same overall geometry of Zn bound to octahedral layer vacancies as measured in the coatings prior to desorption (Figure 2 and Table SI-3 of the Supporting Information) and did not require inclusion of other Zn-bearing phases. These data are consistent with the absence of a secondary Zn phase that could control Zn by a solubility process. Interestingly, increases in Zn_{OCT} from 22 to 30% and in Zn−Mn1 distance of about 0.08 Å for both Zn_{TET} and Zn_{OCT} were observed at pH 5. We hypothesize that vacancy protonation by two H^+ replacing Zn[18] as pH decreases causes expansion of the vacancy from steric effects of two charge-compensating protons bound over a single vacancy. Adjacent vacancies capped with Zn_{TET} or Zn_{OCT} complexes may contract in response to the resulting stress created by protonation of the octahedral sheet. Vacancy contraction would, in turn, cause the Zn tetrahedra and octahdera to move away from the vacancy. The increase in the percentage of Zn_{OCT} in response to the 50% decrease in sorbed Zn is contrary to a previously reported decrease in Zn_{OCT} with the decreased loading and the negligible effect of pH on the fraction of Zn_{OCT}.[17] The presence of other metals and major cations (e.g., Ca^{2+}) in the biogenic Mn oxides formed in the field may account for the difference in the percentage of Zn_{OCT} observed in simpler laboratory systems.

The absence of secondary Zn phases together with the lack of a direct Mn oxide solubility control during desorption and the instability of Zn for incorporation into the birnessite structure[19] are inconsistent with a solubility process controlling Zn desorption that the constant dissolved Zn over the range of solids concentration suggests (Figure 3A). Instead, the observed release of Zn may be the result of a surface complexation process, in which the Zn triple-corner-sharing complex desorbs from the octahedral vacancy sites in exchange for protons or other cations to compensate for the −2 charge on the octahedral vacancy. The observed macroscopic proton stoichiometry of 1.3 indicates that other cations in addition to protons, such as Ca^{2+}, also contribute to the charge compensation required by Zn desorption. The strong correlation between Ca and Mn observed in Pinal Creek Mn oxide coatings[14] indicates that interlayer Ca^{2+} in addition to Mn^{2+} likely accounts for a majority of charge compensation of the vacancies. Sorption data spanning a wider range of conditions (e.g., Zn/Mn ratio, pH, solid concentration, and electrolyte composition) are needed to test if Zn desorption is controlled by surface complexation or dissolution processes. These data would enable development of a surface complexation model that is consistent with the observed tridentate corner-sharing Zn complexes over the octahedral vacancies and the resulting charge compensation required for release of Zn, such as proposed by Appelo and Postma.[39] Additionally, the effect of other sorbed metals and cations present in streamwater (e.g., $Ca^{2+} \sim 10$ mM) and associated with the biogenic Mn oxide needs to be incorporated into the surface complexation model.

Environmental Implications. The co-variation of Zn with Mn in coatings combined with the observed triple-corner-sharing Zn complexes over octahedral vacancies in the biogenic Mn oxide sheet structure are consistent with the observed attenuation of Zn contamination in Pinal Creek occurring largely by sorption to microbial Mn oxides forming during hyporheic exchange. The apparent strong binding of Zn suggests that little desorption would occur in response to a decrease in dissolved Zn inputs to the stream, such as resulting from the ongoing remediation strategy of interception and lime treatment of the contaminated groundwater plume and discharge of neutral pH treated water with low metal concentrations to the stream.[14] However, if the acidic plume reached the perennial streamflow and caused a substantial decrease in streamwater pH, then desorption of the attenuated Zn from the biogenic Mn oxides would occur, resulting in large increases in the dissolved Zn concentration in response to the lower pH. In acidic mine drainages, significant attenuation of Zn and Mn often does not occur until pH increases to near neutral in response to reaction and mixing with uncontaminated water.[40] The strong binding of Zn to octahedral vacancies of biogenic Mn oxides found at Pinal Creek is likely to be an important process in Zn attenuation in the circum-neutral pH reaches of many mine-contaminated streams.

■ ASSOCIATED CONTENT

Ⓢ Supporting Information

Details of sediment coating isolation, desorption experiments, synthesis of SG-1 Mn bio-oxide, XAS measurements and analysis, EXAFS fitting approach, tables of stream and groundwater chemistry, sediment metal concentrations, fitting parameters for Zn EXAFS spectra of sediment samples, Mn K-edge EXAFS of SG-1 bio-oxides, and chalcophanite Zn EXAFS, and figures of μSXRF map of streambed sediment magnetic fraction, Zn reference compound EXAFS spectra, schematic of Zn tridentate surface complex, and dissolved Mn versus pH in desorption experiments. This material is available free of charge via the Internet at http://pubs.acs.org.

■ AUTHOR INFORMATION

Corresponding Author

*Telephone: 650-329-4479. Fax: 650-329-4463. E-mail: ccfuller@usgs.gov.

Notes

The authors declare no competing financial interest.

■ ACKNOWLEDGMENTS

Funding for this work was provided in part by the National Research Program and the Toxics Substances Hydrology Program of the U.S. Geological Survey. Portions of this research were carried out at the SSRL, a Directorate of SLAC National Accelerator Laboratory and an Office of Science User Facility operated for the U.S. Department of Energy (DOE) Office of Science by Stanford University. The SSRL Structural

Molecular Biology Program is supported by the DOE Office of Biological and Environmental Research and the National Institute of General Medical Sciences (NIGMS), National Institutes of Health (NIH) (including P41GM103393). The contents of this publication are solely the responsibility of the authors and do not necessarily represent the official views of NIGMS or NIH. The Advanced Light Source is supported by the Director, Office of Science, Office of Basic Energy Sciences, of the U.S. DOE under Contract DE-AC02-05CH11231. Any use of trade, product, or firm names is for descriptive purposes only and does not imply endorsement by the U.S. Government. Matthew Marcus and Sam Webb assisted with μEXAFS and μSXRF mapping measurements. We thank four anonymous reviewers and J. Peña for helpful comments that improved the manuscript.

REFERENCES

(1) McKenzie, R. M. The adsorption of lead and other heavy metals on oxides of manganese and iron. *Aust. J. Soil Sci.* **1980**, *18*, 61−73.
(2) Balistrieri, L. S.; Murray, J. W. The surface chemistry of sediments from the Panama Basin: The influence of Mn oxides on metal adsorption. *Geochim. Cosmochim. Acta* **1986**, *50*, 2235−2243.
(3) Catts, J. G.; Langmuir, D. Adsorption of Cu, Pb and Zn by δMnO_2: Applicability of the site binding-surface complexation model. *Appl. Geochem.* **1986**, *1*, 255−264.
(4) Shope, C. L.; Xie, Y.; Gammons, C. H. The influence of hydrous Mn−Zn oxides on diel cycling of Zn in an alkaline stream draining abandoned mine lands. *Appl. Geochem.* **2006**, *21*, 476−491.
(5) Tebo, B. M.; Bargar, J. R.; Clement, B. G.; Dick, G. J.; Murray, K. J.; Parker, D.; Verity, R.; Webb, S. M. Biogenic manganese oxides: Properties and mechanisms of formation. *Ann. Rev. Earth Planet. Sci.* **2004**, *32*, 287−328.
(6) Toner, B.; Manceau, A.; Webb, S. M.; Sposito, G. Zinc sorption to biogenic hexagonal-birnessite particles within a hydrated bacterial biofilm. *Geochim. Cosmochim. Acta* **2006**, *70*, 27−43.
(7) Webb, S. M.; Fuller, C. C.; Tebo, B. M.; Bargar, J. R. Determination of uranyl incorporation into biogenic manganese oxides using X-ray absorption spectroscopy and scattering. *Environ. Sci. Technol.* **2006**, *40*, 771−777.
(8) Villalobos, M.; Bargar, J.; Sposito, G. Mechanisms of Pb(II) sorption on a biogenic manganese oxide. *Environ. Sci. Technol.* **2005**, *39*, 569−576.
(9) O'Reilly, S. E.; Hochella, M. F., Jr. Lead sorption efficiencies of natural and synthetic Mn and Fe-oxides. *Geochim. Cosmochim. Acta* **2003**, *67*, 4471−4487.
(10) Peña, J.; Kwon, K. D.; Refson, K.; Bargar, J. R.; Sposito, G. Mechanisms of nickel sorption by a bacteriogenic birnessite. *Geochim. Cosmochim. Acta* **2010**, *74*, 3076−3089.
(11) Lanson, B.; Drits, V. A.; Silvester, E.; Manceau, A. Structure of H-exchanged hexagonal birnessite and its mechanism of formation from Na-rich monoclinic buserite at low pH. *Am. Mineral.* **2000**, *85*, 826−838.
(12) Tonkin, J. W.; Balistrieri, L. S.; Murray, J. W. Modeling sorption of divalent metal cations on hydrous manganese oxide using the diffuse double layer model. *Appl. Geochem.* **2004**, *19*, 29−53.
(13) Fuller, C. C.; Harvey, J. W. Reactive uptake of trace metals in the hyporheic zone of a mining-contaminated stream, Pinal Creek, Arizona. *Environ. Sci. Technol.* **2000**, *34*, 1150−1155.
(14) Bargar, J. R.; Fuller, C. C.; Marcus, M. A.; Brearley, A. J.; Perez De la Rosa, M.; Webb, S. M.; Caldwell, W. A. Structural characterization of terrestrial microbial Mn oxides from Pinal Creek, AZ. *Geochim. Cosmochim. Acta* **2009**, *73*, 889−910.
(15) Lanson, B.; Drits, V. A.; Gaillot, A.-C.; Silvester, E.; Plançon, A.; Manceau, A. Structure of heavy-metal sorbed birnessite: Part 1. Results from X-ray diffraction. *Am. Mineral.* **2002**, *87*, 1631−1645.
(16) Manceau, A.; Lanson, B.; Drits, V. A. Structure of heavy metal sorbed birnessite. Part III: Results from powder and polarized extended X-ray absorption fine structure spectroscopy. *Geochim. Cosmochim. Acta* **2002**, *66*, 2639−2663.
(17) Grangeon, S.; Manceau, A.; Guilhermet, J.; Gaillot, A.-.; Lanson, M.; Lanson, B. Zn sorption modifies dynamically the layer and interlayer structure of vernadite. *Geochim. Cosmochim. Acta* **2012**, *85*, 302−313.
(18) Kwon, K. D.; Refson, K.; Sposito, G. Zinc surface complexes on birnessite: A density functional theory study. *Geochim. Cosmochim. Acta* **2009**, *73*, 1273−1284.
(19) Kwon, K. D.; Refson, K.; Sposito, G. Understanding the trends in transition metal sorption by vacancy sites in birnessite. *Geochim. Cosmochim. Acta* **2013**, *101*, 222−232.
(20) Bargar, J. R.; Tebo, B. M.; Bergmann, U.; Webb, S. M.; Glatzel, P.; Chiu, V. Q.; Villalobos, M. Biotic and abiotic products of Mn(II) oxidation by spores of the marine *Bacillus* sp. strain SG-1. *Am. Mineral.* **2005**, *90*, 143−154.
(21) Villalobos, M.; Lanson, B.; Manceau, A.; Toner, B.; Sposito, G. Structural model for the biogenic Mn oxide produced by *Pseudomonas putida*. *Am. Mineral.* **2006**, *91*, 489−502.
(22) Webb, S. M.; Tebo, B. M.; Bargar, J. R. Structural characterization of biogenic Mn oxides produced in seawater by the marine *Bacillus* sp. strain SG-1. *Am. Mineral.* **2005**, *90*, 1342−1357.
(23) Santelli, C. M.; Webb, S. M.; Dohnalkova, A. C.; Hansel, C. M. Diversity of Mn oxides produced by Mn(II)-oxidizing fungi. *Geochim. Cosmochim. Acta* **2011**, *75*, 2762−2776.
(24) Lanson, B.; Marcus, M. A.; Fakra, S.; Panfili, F.; Geoffroy, N.; Manceau, A. Formation of Zn−Ca phyllomanganate nanoparticles in grass roots. *Geochim. Cosmochim. Acta* **2008**, *72*, 2478−2490.
(25) Marcus, M. A.; Manceau, A.; Kersten, M. Mn, Fe, Zn and As speciation in a fast-growing ferromanganese marine nodule. *Geochim. Cosmochim. Acta* **2004**, *68*, 3125−3136.
(26) Harvey, J. W.; Fuller, C. C. Effect of enhanced manganese oxidation in the hyporheic zone on basin-scale geochemical mass balance. *Water Resour. Res.* **1998**, *34*, 623−636.
(27) Eychaner, J. H. *Solute Transport in Perennial Streamflow at Pinal Creek, Arizona*; United States Geological Survey (USGS): Reston, VA, 1991; USGS Water Resources Investigations Report 91-4034, pp 481−485.
(28) Stollenwerk, K. G. Geochemical interactions between constituents in acidic groundwater and alluvium in an aquifer near Globe, Arizona. *Appl. Geochem.* **1994**, *9*, 353−369.
(29) Kay, J. T.; Conklin, M. H.; Fuller, C. C.; O'Day, P. A. Processes of nickel and cobalt uptake by a manganese oxide forming sediment in Pinal Creek, Globe mining district, Arizona. *Environ. Sci. Technol.* **2001**, *35*, 4719−4725.
(30) Zachara, J. M.; Kittrick, J. A.; Dake, L. S.; Harsh, J. B. Solubility and surface spectroscopy of zinc precipitates on calcite. *Geochim. Cosmochim. Acta* **1989**, *53*, 9−19.
(31) Marcus, M. A.; MacDowell, A. A.; Celestre, R.; Manceau, A.; Miller, T.; Padmore, H. A.; Sublett, R. E. Beamline 10.3.2 at ALS: A hard X-ray microprobe for environmental and materials sciences. *J. Synchrotron Radiat.* **2004**, *11*, 239−247.
(32) Best, J. E.; Geiger, K. E.; O'Day, P. A. *Partitioning of Trace Metals between Contaminated Stream Waters and Manganese Oxide Minerals, Pinal Creek, Arizona*; United States Geological Survey (USGS): Reston, VA, 1999; USGS Water Resources Investigations Report 99-4018A, Vol. *1*, pp 227−237.
(33) Waychunas, G. A.; Fuller, C. C.; Davis, J. A. Surface complexation and precipitate geometry for aqueous Zn(II) sorption on ferrihydrite I: X-ray absorption extended fine structure spectroscopy analysis. *Geochim. Cosmochim. Acta* **2002**, *66*, 1119−1137.
(34) Trainor, T. P.; Brown, G. E., Jr.; Parks, G. A. Adsorption and precipitation of aqueous Zn(II) on alumina powders. *J. Colloid Interface Sci.* **2000**, *231*, 359−372.
(35) Bochatay, L.; Persson, P. Metal ion coordination at the water−manganite (γ-MnOOH) interface: II. An EXAFS study of zinc(II). *J. Colloid Interface Sci.* **2000**, *229*, 593−599.
(36) Li, X.; Pan, G.; Qin, Y.; Hu, T.; Wu, Z.; Xie, Y. EXAFS studies on adsorption−desorption reversibility at manganese oxide−water

interfaces: II. Reversible adsorption of zinc on δ-MnO_2. *J. Colloid Interface Sci.* **2004**, *271*, 35−40.
(37) Tani, Y.; Ohashi, M.; Miyata, N.; Seyama, H.; Iwahori, K.; Soma, M. Sorption of Co(II), Ni(II), and Zn(II) on biogenic manganese oxides produced by a Mn-oxidizing fungus, strain KR21-2. *J. Environ. Sci. Health, Part A: Toxic/Hazard. Subst. Environ. Eng.* **2004**, *39*, 2641−2660.
(38) Lefkowitz, J. P.; Rouff, A. A.; Elzinga, E. J. Influence of pH on the reductive transformation of birnessite by aqueous Mn(II). *Environ. Sci. Technol.* **2013**, *47*, 10364−10371.
(39) Appelo, C. A. J.; Postma, D. A consistent model for surface complexation on birnessite (−MnO_2) and its application to a column experiment. *Geochim. Cosmochim. Acta* **1999**, *63*, 3039−3048.
(40) Kimball, B. A.; Walton-Day, K.; Runkel, R. L. Quantification of metal loading by tracer injection and synoptic sampling, 1996−2000. In *Integrated Investigations of Environmental Effects of Historical Mining in the Animas River Watershed, San Juan, County, Colorado*; Church, S. E., von Guerard, P., Finger, S. E., Eds.; United States Geological Survey (USGS): Reston, VA, 2007; USGS Professional Paper 1651, pp 423−495.